Grand canonical Monte Carlo simulations of the distribution and chemical shifts of xenon in the cages of zeolite NaA. I. Distribution and ^{129}Xe chemical shifts

Cynthia J. Jameson
Department of Chemistry, University of Illinois at Chicago, M/C 111, Chicago, Illinois 60607-7061

A. Keith Jameson
Department of Chemistry, Loyola University, Chicago, Illinois 60626

Bernoli I. Baello and Hyung-Mi Lim
Department of Chemistry, University of Illinois at Chicago, Chicago, Illinois 60607-7061

(Received 17 November 1993; accepted 30 December 1993)

The equilibrium distribution of the Xe atoms among the alpha cages of the zeolite NaA have been measured directly by nuclear magnetic resonance (NMR) in ten samples ranging from very low xenon loading up to saturation. These distributions are simulated by a grand canonical Monte Carlo (GCMC) method which reproduces the experimental data quantitatively for all ten samples at 296 K and also at 360 K. The adsorption isotherm of the high loading samples has been determined directly from the chemical shift of the gas in equilibrium with the adsorbed xenon. The data compare favorably with the adsorption isotherms resulting from the simulations. The previously reported ^{129}Xe chemical shifts of the individual Xe_n clusters and their temperature dependences in the range 188–420 K are reproduced quantitatively by the GCMC simulation which makes use of pairwise additive *ab initio* intermolecular shielding functions. These cluster shifts and their temperature dependence encode the distribution of configurations for a given Xe_n cluster in an alpha cage. Quantitative agreement with the three experimental measures of the distribution of Xe atoms in NaA (partitioning between the adsorbed phase and the gas phase, distribution of the intrazeolitic atoms among the alpha cages, and the distribution of Xe atoms within an alpha cage containing Xe_n) as a function of temperature has been achieved for the first time.

I. INTRODUCTION

Microporous solids are widely used in heterogeneous catalytic processes, separations, oil recovery, and other industrial processes.[1] These applications depend on a large number of microscopic processes, among which are adsorption and diffusion. Understanding the role of confined geometry on the dynamic behavior of molecules in these microporous solids is not only relevant to the technological applications, but is also fundamentally interesting. Zeolites, consisting of AlO_4 and SiO_4 tetrahedra linked together in such a way as to form cages of 3–13 Å diameter, connected in a continuous network of pores extending in one, two, or three dimensions, are widely used in the applications that depend on their properties as shape-selective catalysts or adsorbents.[2–7] Based on the large nuclear magnetic resonance (NMR) chemical shifts of the ^{129}Xe nucleus and the previously observed large effects of intermolecular interactions in the gas phase,[8–11] and in solutions,[12,13] Fraissard's pioneering work on Xe adsorbed in zeolites has made ^{129}Xe NMR spectroscopy a popular technique for characterizing zeolites, polymers, and various microporous solids.[14,15] What is generally observed in the ^{129}Xe NMR spectrum of xenon adsorbed in a zeolite is a single peak, with a resonance frequency that changes with xenon loading. Loading is usually expressed in terms of the number of Xe atoms/g zeolite and is based on independently measured adsorption isotherms. In simple zeolites this is usually converted to $\langle n \rangle$, the average number of Xe atoms per cavity.[16] The ^{129}Xe chemical shift inside a zeolite in the zero loading limit, is found to be characteristic of the zeolite and is roughly indicative of the size of the cavities.[14,17] The magnitude of the change of the chemical shift with $\langle n \rangle$ is also found to be characteristic of the zeolite type. Most experiments have been in the range of loadings equivalent to $\langle n \rangle = 0-2.5$ Xe atoms/cavity. Occasionally, very high loading had been obtained by lowering the temperature, but this sometimes leads to problems of nonreproducible spectra when an equilibrium distribution of Xe atoms is not achieved since the mobility of xenon is substantially reduced at low temperatures.[18] Changes in the ^{129}Xe chemical shifts due to the presence of other guest molecules in the cavities has raised the possibility of using Xe NMR as a means of characterizing the intrazeolitic distribution of the guest molecules.[19,20]

It is generally agreed that in the limit of zero loading, the ^{129}Xe chemical shift varies roughly inversely with the cavity size. There are several linear relationships that have been used to relate this ^{129}Xe chemical shift in a single Xe atom interacting with the internal surface of the zeolite to some measure of the pore diameter.[21–24]

For low loading of Xe in zeolites, the ^{129}Xe chemical shift is generally found to increase with increasing $\langle n \rangle$, with rare exceptions. The shapes of the curves of ^{129}Xe chemical shift vs $\langle n \rangle$ depend on the type of zeolite in an unpredictable way; some are linear, others are not. Generally, they are concave upward, i.e., the increase of the ^{129}Xe chemical shift with the average number of Xe atoms per cavity becomes more pronounced with higher loading. These curves serve as

fingerprints of zeolite types; they are more or less reproducible in various laboratories but they are not predictable, *a priori*, from zeolite structure. Although it might be suspected that these curves are largely dependent on Xe–Xe interactions, their shapes are not the same as that observed in dense Xe gas samples, and they do depend on the zeolite type. What has been missing so far is a quantitative physical interpretation of these observations.

Our work is different from others in that we use sealed samples containing an overhead pressure of Xe gas in every case. We can determine, directly from the chemical shift of the ^{129}Xe nuclei in this free Xe gas over the zeolite, the density of the Xe gas in equilibrium with the Xe inside the zeolite cages. We calculate $\langle n \rangle$ directly from a mass balance of Xe in the sample. The relationship between the average number of Xe atoms per cage and the density of the overhead gas is an adsorption isotherm, which we directly obtain by NMR. The range of measurements we are able to carry out is much greater than the range of studies reported in the literature. We have presented the first report ever of ^{129}Xe chemical shifts in a zeolite for the entire range of loading, i.e., up to saturation, under conditions where equilibrium is definitely achieved.[25,26]

Toward a fundamental understanding of sorption in micropores, detailed information on adsorbate distribution, site occupancy within a cage, rates of site-to-site exchange, cage-to-cage transfer, translation, and reorientation dynamics are extremely important. Computer simulations provide detailed information at the molecular level but these simulations have not been adequately tested by comparisons with experiment. Only limited experimental information such as adsorption isotherms or diffusion coefficients are sometimes available. For example, consider adsorbate distributions. What is the equilibrium distribution of sorbate molecules in a given microporous solid? What factors influence this distribution? Until recently, no direct measure of the distribution of molecules in zeolite cavities or other pores was available. By counting the minimum number of protons that are spin–spin interacting with each other, Pines *et al.* conclusively demonstrated, using multiple quantum NMR spectroscopy, that some cavities in zeolite NaY contained as many as two molecules of hexamethylbenzene (as many as 38 protons were detected) at a loading of 20 wt. %, but only one molecule per cavity at a loading of 10% or less.[19] Pines *et al.* observed the equilibrium distribution of Xe in zeolite NaA at 523 K,[27] and in our recent work,[25] we directly observed the distribution of xenon atoms in the alpha cages of zeolite NaA by high-resolution FTNMR spectroscopy; i.e., we measured directly the fraction of alpha cages containing none, one, two, three,..., eight xenon atoms, as a function of loading and temperature in samples which were at equilibrium at room temperature (and also at 360 K).[25] Detailed information of this sort provides critical tests of computer simulations.

We found that the experimental distributions differ from the strictly statistical distributions of hard-sphere atoms in mutually exclusive specific lattice sites (hypergeometric distribution)[28] or the statistical distribution of freely moving hard spheres in alpha cages with no specific sites (continuum model).[29] The experimental deviations from these statistical models can be explained by the attractive Xe–Xe interactions which favor clustering at modest loading, and the higher energy associated with the overcrowded cage disfavoring clusters of eight Xe atoms at high loadings.

Because we observe the free gas in equilibrium with the intrazeolitic sorbate, we also measure the adsorption isotherm by NMR. Furthermore, since singles (one Xe atom in a cavity) and clusters of two up to eight atoms are individually observed in the ^{129}Xe spectrum, we have been able to measure the temperature dependence of the ^{129}Xe chemical shift of each cluster in the range 188–420 K.[25] The average chemical shift observed for a given cluster and its temperature dependence encodes the information about adsorption site occupancy and the one-body distribution function inside an alpha cage for the single Xe atom. For clusters Xe_2, Xe_3,...,Xe_8 the average chemical shift further encodes the pair distribution function within the cluster, and the distributions of the various n-body configurations, since the observed chemical shifts are entirely due to intermolecular effects. In simple terms, the chemical shift contains the information about all the close encounters between the Xe and Xe, as well as Xe and zeolite atoms (primarily O atoms and Na^+ ions). The ^{129}Xe chemical shifts are a very stringent test of any computer simulation. Since the shifts are measured relative to a well-defined reference, the free Xe atom, then no adjustment is permissible; the shifts have been measured absolutely. There are extremely interesting features of these shifts, such as the incremental shift increasing slightly in going from Xe_1 to Xe_6 and the big incremental shift (44 ppm) in going from Xe_6 to Xe_7 and also from Xe_7 to Xe_8. Furthermore, the temperature dependences are systematically changing with increasing cluster size, with the slope being negative for Xe_1 and increasing systematically algebraically with cluster size. Xe_7 and Xe_8 have large positive temperature coefficients. These are strongly inhomogeneous systems since the density varies significantly over molecular dimensions. The Xe chemical shift is our probe of just these density fluctuations within the alpha cage.

Thus, from our experiments we have directly observed several of the quantities which can be provided by a computer simulation: (a) the fractions of alpha cages containing zero, one, two, three,..., eight Xe atoms for a given average occupancy or xenon loading, $\langle n \rangle$; (b) the adsorption isotherm; (c) the chemical shifts of each cluster; and (d) their temperature dependences. We believe that an understanding of the details of how the Xe atoms behave within the zeolite NaA cavities can be said to be achieved if these observations can be reproduced by the computer simulations within experimental error.

Well-established molecular dynamics (MD) simulations and Monte Carlo techniques have been applied to the motion of xenon atoms within zeolites in several laboratories: in zeolites NaX and NaY (Refs. 30–34) and in silicalite,[35,36] using potential functions that are largely based on the work of Kiselev and Du.[37,38] van Tassel *et al.* have done canonical ensemble Monte Carlo simulations of Xe in a model cage containing framework atoms on the vertices and line segments of a truncated cuboctahedron[39] and in an idealized NaA-type framework: cations are located in the six rings and

in the centers of the eight rings (contrary to the x-ray structure) in their "cation-rich" model.[40] These results, surprisingly, allow as many as 24 Xe atoms in the alpha cage. More recently (after this work was completed), molecular dynamics simulations of Xe in zeolite rho[41] and grand canonical simulations of xenon in NaA (Ref. 42) have appeared.

In this paper we report new experimental data on xenon in zeolite NaA: the fractions $f(n)$ of the alpha cages containing n=zero, one, two,..., eight Xe atoms for average occupancies ranging from 0.45 Xe atoms per cage to 6.73 Xe atoms per cage in samples that are in equilibrium with the gas phase at room temperature. We report the distribution of the xenon between the gas phase and the intrazeolitic cavities (the adsorption isotherm). These experimental measures of the xenon distribution augment the information on the distribution of the n Xe atoms within one alpha cage that has been encoded in the ^{129}Xe chemical shifts reported earlier. We report grand canonical Monte Carlo simulations of this system, which reproduce the observed equilibrium distributions of the xenon atoms, the chemical shifts of the Xe_1, Xe_2,...,Xe_8 clusters, and their temperature dependences.

II. EXPERIMENT

The details of sample preparation and data analysis are described elsewhere.[25] We outline briefly the nature of the information obtained. In the sealed samples of Xe in dehydrated zeolite NaA the density of the gas in equilibrium with the xenon inside the zeolite is determined from the measured resonance frequency of the gas peak, through our well-established ^{129}Xe chemical shift vs density and temperature relations in the pure xenon gas. This provides a measure of the adsorption isotherm and from a xenon mass balance this allows us to deduce the equilibrium average number of Xe atoms per cavity $\langle n \rangle$ by difference. For a given sample, the intensities of the peaks in typical NMR spectra such as shown in Fig. 1 provide a direct measure of the fractions of the alpha cages that have one, two, three,..., eight Xe atoms, and the fraction that are empty are known by difference, since $\langle n \rangle$ is obtained independently. Where there are no empty cages, at sufficiently high loading, we obtain $\langle n \rangle$ directly from peak intensities, which provides an independent check on the $\langle n \rangle$ obtained from mass balance. The NMR spectrum thus provides not only the adsorption isotherm but a direct measure of the distribution of Xe atoms among the alpha cages of dehydrated zeolite NaA. Ten samples with $\langle n \rangle$ spanning the range of values from $\langle n \rangle = 0.449$ to $\langle n \rangle = 6.73$ at room temperature have been studied in this manner and the fractions $f(n)$ of alpha cages containing Xe_n have been directly measured in each of the ten samples. Of these ten, six were prepared using ^{129}Xe-enriched xenon (99%, ICON, Mt. Marion, NY). The others, with xenon at natural abundance, had been used in the previous work.[25] We therefore have a significant body of experimental data to test any simulation of the system.

The chemical shifts of the individual clusters Xe_n have been measured as a function of temperature. They are found to be independent of the sample or the xenon loading.

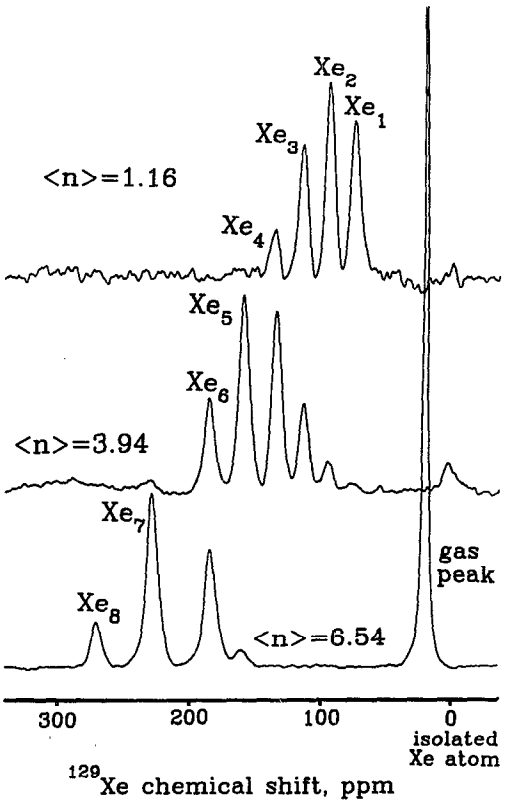

FIG. 1. Typical NMR spectra obtained for sealed samples of xenon in dehydrated zeolite NaA which are at equilibrium at 296 K.

III. THE MODEL

A unit cell of dehydrated zeolite NaA has the composition $\{Na_{12}[(AlO_2)_{12}(SiO_2)_{12}]\}_8$. In the simulations the framework is represented by the $Fm\bar{3}c$ space group (a=24.555 Å). Each unit cell contains eight large cavities (alpha cages) and eight small ones (beta cages). The unique set of coordinates of the framework atoms are taken from the x-ray diffraction studies on the dehydrated zeolite.[43] The oxygen atoms bridging the Si and Al atoms form rings with four, six, and eight oxygens. In the pseudounit cell, 8 of the 12 Na^+ ions occupy positions in the 8 six-rings [labeled Na(I)], one is in the alpha cage in a one-sided square pyramidal coordination with a four-ring [Na(III)]. The other three Na^+ ions are off-centered in the six windows formed by the eight-rings [Na(II)]. (See Fig. 2.) There is a transition from the rhombohedral symmetry ($R\bar{3}c$ by neutron diffraction at 4.5 and 296 K) to the cubic symmetry at 335 K.[44] Above the transition, neutron diffraction results[44] are in agreement with the x-ray single crystal refinements of Pluth and Smith.[43] Below the transition, neutron diffraction indicates that ordering of the Na(II) ions takes place. There are four equivalent off-center sites for Na(II) in the eight-ring window. Above 335 K they have 1/4 occupancies. It has been shown by neutron diffraction data[44] that the rhombohedral symmetry observed at room temperature and below can be attributed to ordering of Na(II) ions into two of the four positions, with otherwise no relaxation of the $Fm\bar{3}c$ positional constraints on any of the framework atoms or the distribution of the Na^+ ions among

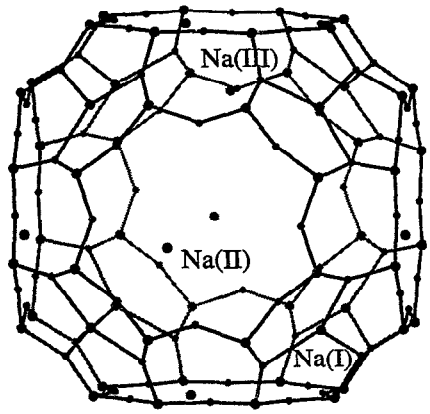

FIG. 2. A schematic representation of an alpha cage of zeolite NaA. The atoms are designated by small spheres located at the positions according to the x-ray diffraction results (Ref. 43). The Na ions in the sites labeled I are shown coordinated to three oxygen atoms that form a six-oxygen ring. The Na ions in the sites labeled II are located off-centered in each of the eight-oxygen ring windows. Their coordination to three oxygens of the eight-ring is not shown in this diagram. There is one Na ion in site III, located inside the alpha cage, forming a one-sided coordination (not shown) with a four-ring.

the three types. Therefore, we placed the Na(II) ions in the window sites according to the complete ordering on one of these two sites. The coordinates for the atoms in the unit cell are generated from the unique set by applying the symmetry operations of the $Fm\bar{3}c$ space group.[45] The lattice is assumed to be rigid in the simulations; we will neglect vibrations of the framework atoms and ions at this time.

The potential function for the interaction of the xenon with the zeolite is assumed to be the pairwise additive effective potential in which only the Xe–O and Xe–Na^+ pairs are included, and these are parametrized following Woods and Rowlinson for Xe in zeolite NaX and NaY.[46] We assume that pairwise additive interactions adequately describe the interactions of Xe with the surface. Surface-mediated indirect interactions between adsorbates is at least a three-body term and is probably not very important for physisorbed species. Schmeits and Lucas[47] have predicted that these indirect interactions have both attractive and repulsive parts, depending on the regions in the cage occupied by the adsorbates. The most important three-body terms probably involve three Xe atoms. We will neglect this. We regard pairwise additivity as a useful approximation and use this assumption to generate the model functions for the potential energy and shielding surfaces at arbitrary loading. The total potential energy of xenon atoms is represented by a sum over all Xe–Xe pairs and Xe with all lattice oxygens and Na^+ ions, with the cut-off distance of half the lattice parameter. The Si and Al atoms are neglected in the potential summation. We made only a minor modification in the Woods and Rowlinson Xe–O Lennard-Jones parameter from $r_0=3.27$ Å to $r_0=3.37$ Å and an accompanying change in the ϵ so as to leave unchanged the area in the bowl in the cut-shifted Xe–O potential. This minor change altered the effective size of the alpha cage so that Xe_9 is rarely observed in the simulation even at the highest loading, in agreement with observation. The parameters used for the Xe–zeolite potential are listed in Table I. The Xe–Xe potential we used is not the usual Lennard-Jones form used by Woods and Rowlinson and others, for the following reasons. In calculating the average chemical shift, we need the ^{129}Xe shielding function, i.e., the nuclear shielding of a ^{129}Xe nucleus in a xenon atom interacting with another Xe atom at a distance r from it. The largest contributions to the average chemical shift come from the Xe–Xe encounters. We know this from having observed Xe chemical shifts in mixtures of xenon with other gases, including polar molecules such as HCl or large molecules such as SF_6. The Xe–Xe contributions are the largest we found.[8] Therefore, the Xe–Xe shielding function has to be properly sampled if the ^{129}Xe chemical shifts in zeolites are to be predicted correctly. We have a shielding function $\sigma(r)$ that reproduces the second virial coefficient σ_1 of the ^{129}Xe chemical shift in pure xenon gas,[51] i.e.,

$$\sigma_1=\int_0^\infty 4\pi r^2\, dr[\sigma(r)-\sigma(\infty)]\exp[-U(r)/kT]. \qquad (1)$$

The shielding function $[\sigma(r)-\sigma(\infty)]$ is negative and decreases sharply with r, roughly going as r^{-6} for the rare gases.[48] This means that in the simulation, when the infrequently sampled short Xe–Xe separations do contribute, they contribute large chemical shifts. Therefore, the Xe–Xe potential that we use in the simulation has to be particularly accurate for those r values where the $[\sigma(r)-\sigma(\infty)]$ changes rapidly. For this simulation we cannot use the usual Xe–Xe Lennard-Jones function that has r_0 at 4.1 Å in contrast to the best Xe–Xe potential that has an r_0 at 3.892 44 Å. The Aziz–Slaman potential[49] is of the Hartree–Fock damped form (HFD-B) and appears to be the best characterization of the Xe–Xe interaction, reproducing within experimental errors virial coefficients, viscosities, and thermal conductivities over a wide temperature range. It also predicts within experimental error molecular beam scattering, differential cross sections, total cross sections, and the vibrational spacings of the Xe dimer. This potential is given below:

$$\begin{aligned} U(r)&=\epsilon A\exp(-\alpha\bar{r}+\beta\bar{r}^2) \\ &\quad -F(\bar{r})[C_6\bar{r}^{-6}+C_8\bar{r}^{-8}+C_{10}\bar{r}^{-10}], \\ F(\bar{r})&=\exp\left[-\left(\frac{D}{\bar{r}}-1\right)^2\right] \quad \text{for } \bar{r}<D \quad \text{and} \quad 1 \quad \text{for } \bar{r}\geq D, \end{aligned} \qquad (2)$$

where $\bar{r}$ is $r/r_{\min}$. The values of the parameters are given in the original reference.[49] r_0 is 3.892 44 Å, r_{min}=4.3627 Å, and ϵ/k is 282.29 K. This form is too complex to use in a simulation where the potential energy is calculated for all Xe–Xe pairs at each of the million or more cycles in the

TABLE I. The Lennard-Jones parameters used for the pairwise potentials that are used here to model the Xe–zeolite interaction.

	r_0 (A)	ϵ/k (K)	Reference
Xe–O	3.37[a]	217.0	
Xe–Na^+	3.676	39.08	46

[a]Modified from $r_0=3.27$ Å from Ref. 46. The ϵ/k value preserves the area in the bowl of the cut-and-shifted potential from Ref. 46.

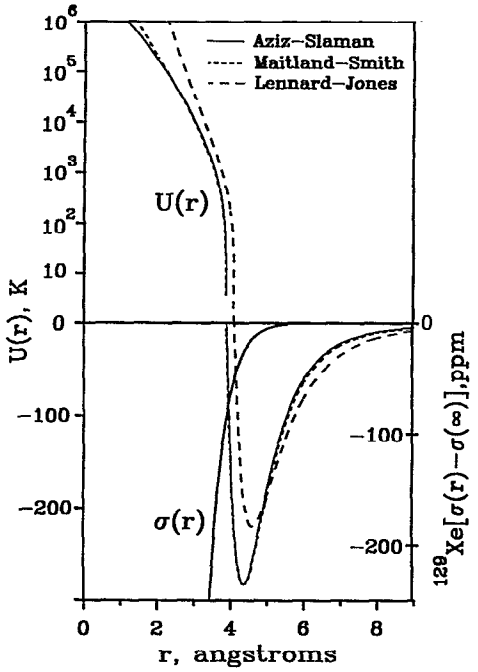

FIG. 3. Xe–Xe potential functions. The Maitland–Smith function is a best representation of the Aziz–Slaman function (see the text) which is just as convenient to use in a Monte Carlo simulation as the Lennard-Jones form. The Lennard-Jones function shown here is the one used in all previous simulations of Xe in zeolites (references cited in the text). Also shown is the ^{129}Xe shielding function from Ref. 51 which reproduces the chemical shifts in pure xenon gas.

simulation. Therefore, we followed a suggestion by Smith to use the Maitland–Smith potential form, as follows:

$$U(r)=\epsilon\left\{\frac{6}{n-6}\ \bar{r}^{-n}-\frac{n}{n-6}\ \bar{r}^{-6}\right\}, \tag{3}$$

where n is allowed to vary with $\bar{r}$ according to

$$n=m+\gamma(\bar{r}-1),$$

where we take the $r_{\min}$ and ϵ/k from Aziz–Slaman and use the recommended parameter values $m=13$ and $\gamma=11$.[50] Figure 3 shows the Maitland–Smith, the Aziz–Slaman, and the commonly used Lennard-Jones ($r_0=4.1$ Å and $\epsilon/k=221$ K) potentials for Xe–Xe. It can be seen in this figure that the Lennard-Jones potential would offer very poor sampling of the shielding function at the short distances where the shielding function is most significant.

For the Xe–zeolite shielding function we used approximate models. Since the intermolecular nuclear magnetic shielding is a very local property, we used as a first approximation pairwise contributions from $\sigma(\text{Xe–O}_{\text{zeol}})$ and $\sigma(\text{Xe–Na}^+_{\text{zeol}})$ terms. The form of the $\sigma(\text{Xe–O}_{\text{zeol}})$ shielding function should not significantly compromise the chemical shift between clusters. *Ab initio* calculations on the ^{39}Ar shielding in the model systems Ar–OH_2 and Ar–Na^+ were used to construct the $\sigma(\text{Xe–O}_{\text{zeol}})$ and $\sigma(\text{Xe–Na}^+_{\text{zeol}})$, respectively. The scaling of the $\sigma(^{39}\text{Ar in Ar–Na}^+)$ to the $\sigma(^{129}\text{Xe in Xe–Na}^+)$ was carried out in the same way as the scaling for the rare gas pairs, the scaling factors for the shielding are discussed in Ref. 51, involving only the fundamental electronic properties, polarizabilities, and the ionization potentials and the $\langle a_0^3/r^3\rangle$ for the rare gas atoms. The resulting $\sigma(^{129}\text{Xe in Xe–O}_{\text{zeol}})$ and the $\sigma(^{129}\text{Xe in Xe–Na}^+_{\text{zeol}})$ functions are scaled in r in the same manner as the $\sigma(^{129}\text{Xe in Xe–Xe})$ function.

Our model then is a rigid zeolite lattice with the framework atoms located at the positions obtained from x-ray and neutron diffraction, including the Na^+ ions, with pairwise additive energies of interaction between Xe atoms, and pairwise additive shielding contributions to a ^{129}Xe in the vicinity of other Xe atoms. The Xe–Xe pair potential is represented by a Maitland–Smith function which mimics the best Xe–Xe pair potential for the gas phase, and the intermolecular shielding function is that derived from *ab initio* calculations scaled to Xe–Xe, and which reproduces the second virial coefficient of the NMR chemical shifts in pure xenon gas. The Xe–zeolite interactions are likewise assumed to be sums of pair interactions, with the Si and Al atoms not included in the sums, using effective Xe–O and Xe–Na^+ potentials of the Lennard-Jones form taken from Woods and Rowlinson's simulations of Xe in zeolite NaX and NaY.[46] The zeolite contribution to the Xe chemical shift is assumed to be pairwise sums just like the energy sums, except summing over terms from shielding functions rather than potential functions. The potential functions and the shielding functions are all cut-and-shifted in the usual manner, i.e.,

$$\begin{aligned} U(r_{ij})&=U(r_{ij})-U(r_e), \quad r_{ij}\leqslant r_c \\ &=0, \qquad\qquad\quad r_{ij}>r_c, \end{aligned} \tag{4}$$

where r_c is the cut-off radius, similar for the shielding function. The simulation box is one unit cell which has eight alpha cages and eight beta cages; periodic boundaries and the minimum image convention are used. Consistent with this is the choice of cut-off radius equal to half the lattice parameter. To simulate the adsorption isotherm and the equilibrium distribution of the Xe atoms among the cages of the zeolite at any given temperature, we carry out a grand canonical Monte Carlo simulation. The chemical potential and the temperature are fixed while the number of molecules fluctuates. The GCMC techniques have been described thoroughly by Allen and Tildesley.[52] We follow the procedures used in the previous studies by Woods and Rowlinson.[30,31,46] The initial configuration was taken from a large standard random configuration previously generated by inserting one molecule at a time into the unit cell and accepting it if the total energy of the system was less than zero. A number of GCMC cycles were discarded so that equilibrium could be attained before the simulation data are acquired. For the results reported here 10^5 cycles were discarded before the simulation proper. The Norman–Filinov technique is used:[53] a displacement step is followed by two-particle creation or annihilation attempts. The attempted move is immediately rejected if it would cause any obvious overlap with other adsorbed molecules or zeolite atoms, otherwise the move is accepted with a probability P_{acc} given by[31]

$$P_{\text{acc}}=\begin{cases}\min[1,\exp(-\Delta E/kT)], & \Delta E/kT\leqslant 180 \\ 0, & \Delta E/kT>180\end{cases}, \tag{5}$$

where ΔE is

create: $$\Delta E=\Delta U_{ji}(\mathbf{r}^N)+kT\ \ln[(N+1)/V\rho^0]-\mu; \tag{6}$$

annihilate: $$\Delta E=\Delta U_{ji}(\mathbf{r}^N)+kT\ \ln[(N)/V\rho^0]+\mu; \tag{7}$$

displace: $$\Delta E=\Delta U_{ji}(\mathbf{r}^N); \tag{8}$$

in which the configurational energy change is

$$\Delta U_{ji}(\mathbf{r}^N)=U_j(\mathbf{r}^N)-U_i(\mathbf{r}^N),$$
$$\text{NEW} \quad \text{OLD}. \tag{9}$$

μ is the imposed value of the configurational chemical potential, V is the volume of the unit cell, N is the number of molecules in the unit cell at a given instance, and ρ^0 is a standard density of 1 Å^{-3}.

The information about the structure of the adsorbed fluid at some average number of Xe atoms per unit cell, $\langle N\rangle$, is collected in the form of an average one-body distribution function obtained by dividing the unit cell into $80\times80\times80$ smaller cubes and counting how many configurations placed the center of a xenon atom in each cube. The structure of the individual clusters inside an alpha cage, Xe_1, Xe_2, Xe_3,...,Xe_8, were obtained in the same way. The pair distribution functions for a given $\langle N\rangle$ were collected, as were the pair distribution functions for each cluster. The distribution of occupancies in the unit cell and the distribution of occupancies in a single alpha cage were obtained. Each simulation of typically 9×10^5 cycles was divided into blocks of typically 10^5 cycles each. The average values of properties are obtained from the entire simulation and the statistical errors are determined from the mean-square deviations of the block averages. The average shielding of each cluster at a given temperature is found to be independent of the average number of Xe atoms per unit cell, so all cluster shieldings from all simulations at the same temperature could be pooled together to provide average shielding values for each Xe_n at that temperature.

At high loadings the GCMC method will give poor results for fluctuation quantities $f(n)$ and $F(N)$ because of the very small number of acceptances for the creation and annihilation steps. As suggested by Woods and Rowlinson,[31] we adjust the step size for the displacement steps according to the acceptance ratio, using 50% acceptance as the desirable value. Creation and annihilation steps pose a problem at very high loadings in that creation attempts fail because of the high probability of overlap with other Xe atoms and annihilation attempts fail because removing a molecule without allowing the fluid structure to relax results in the loss of attractive interactions. Mezei has shown that the average density (and hence other average properties) is quite accurate even when the acceptance ratio for particle creation/annihilation steps may be as low as 0.1%,[54] but even so, at very high loadings configurations become "locked in," and adding more cycles does not help. For these very high loadings we may improve the precision by averaging over several complete GCMC runs rather than simply increasing the number of cycles by the same factor. Nevertheless, the fluctuation quantities such as $f(n)$ would be less precise at low acceptance ratios. The equation of state for xenon gas was solved numerically for the density and pressure corresponding to a given value of the chemical potential and temperature, in order to generate the adsorption isotherms. The equation of state used is the modified Benedict–Webb–Rubin equation with 32 parameters.[55] The chemical potential at a density ρ and temperature T is given by[46]

$$\mu_{\text{gas}}=kT\ \ln(\rho/\rho^0)+kT(Z-1)+\int_0^\rho d\rho(P-kT\rho)/\rho^2, \tag{10}$$

where Z is the compressibility factor.

All calculations reported here were carried out on an IBM RISC/6000 model 560.

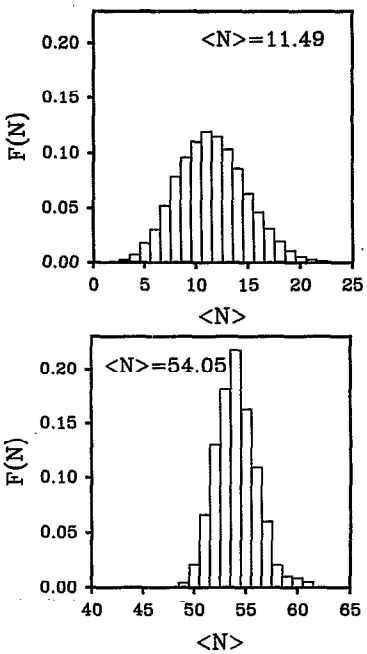

FIG. 4. Distribution of the xenon atoms among the unit cells of the zeolite NaA. $F(N)$ is the fraction of the unit cells that have N Xe atoms, shown here for $\langle N\rangle=11.49$ and $\langle N\rangle=54.05$ at 300 K.

IV. RESULTS

A. Distribution of xenon atoms among the alpha cages and in the gas phase

We consider first the distribution of occupancies of the unit cells. $F(N)$ is the fraction of the unit cells that have N Xe atoms. As was also found by Woods and Rowlinson[31] for Xe in zeolite NaX and NaY, the distributions of occupancies in the unit cell are fairly broad and quite symmetric around the most probable occupancy at low to medium occupancies, and narrows significantly at very high occupancies. Two examples are shown in Fig. 4. We are convinced that this broadness of the distributions is a general feature of the adsorption in zeolites. The much narrower distributions of occupancies at very high loadings for trapped Xe in NaA is different from the findings in the more open networks of NaY and CaA.

Of greater interest are the distribution of occupancies in the alpha cages for these can be compared directly with our

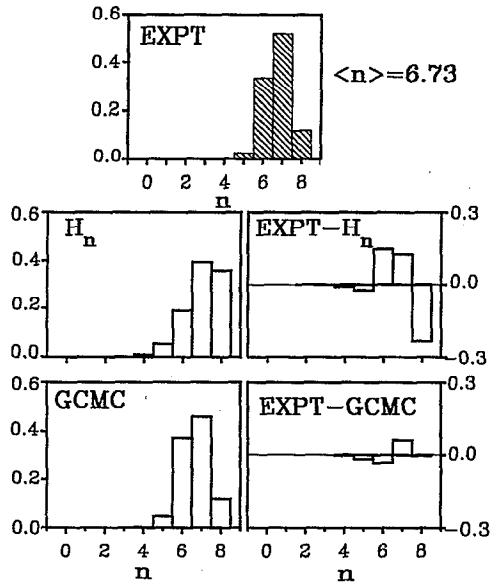

FIG. 5. A comparison of the experimental equilibrium distribution of xenon atoms among the alpha cages of zeolite NaA at $\langle n\rangle = 6.73$ with the strictly statistical distribution (hypergeometric distribution) H_n and the distribution resulting from a GCMC simulation. The histograms display the fractions of the alpha cages that have zero, one, two,..., eight Xe atoms.

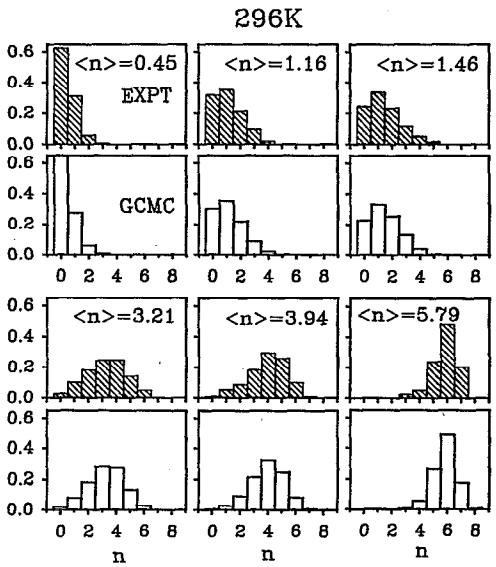

FIG. 6. The $f(n)$, the fractions of the alpha cages that have zero, one, two, three,..., eight xenon atoms, measured directly from the NMR spectrum of samples at equilibrium at 296 K, having $\langle n\rangle = 0.45$ up to 5.79 Xe atoms per cage on the average. The GCMC results for the chemical potential such that the resulting value of $\langle n\rangle$ are very close to the experimental ones are shown here for comparison.

measurements in ten samples. It had been shown in our previous work[25] that strictly statistical distributions do not agree well with our experimentally observed distributions. We show one example in Fig. 5, a comparison of a statistical distribution (the hypergeometric distribution) and the distribution obtained from the GCMC simulations at a chemical potential such that the $\langle n\rangle$ is very close to the experimental one. These histograms are the fractions of alpha cages containing $n = 4, 5, 6, 7, 8$ Xe atoms. The statistical distribution is definitely not in agreement with the experiment whereas the GCMC results mimic the experimental data quite well. Other examples illustrating the deviations from the hypergeometric distribution for Xe in NaA have been published previously.[25] Figures 6 and 7 show the distributions in the form of histograms, the fractions of alpha cages containing zero up to eight Xe atoms for ten samples, with xenon loadings varying from 0.45 Xe atoms per alpha cage to 6.73 Xe atoms per alpha cage, at 296 K. In Fig. 7 is also shown two of these samples at 360 K. The sample shown with $\langle n\rangle = 0.89$ at 360 K is physically the same sample that had $\langle n\rangle = 1.46$ at 296 K, and the sample with $\langle n\rangle = 6.28$ at 360 K is the same sample that had $\langle n\rangle = 6.73$ at 296 K. In each of these comparisons, the GCMC result is for a chemical potential such that the simulated $\langle n\rangle$ is closest to the experimental $\langle n\rangle$. The agreement of the simulation results with the experimental data is very good for all ten samples at 296 and 360 K. These samples cover a very wide range of loading conditions, from low loading to near saturation.

An earlier report of the distributions of Xe atoms in the cages of zeolite NaA was for samples which were prepared at 523 K and quenched.[27] After some time, the NMR spectra of these samples were observed at room temperature, from which intensities the $f(n)$ were calculated. These samples might then be considered to have the equilibrium distributions characteristic of 300 K. We have taken the $f(n)$ from the figures in Ref. 27 and find that these $f(n)$ do correspond to their reported values of $\langle n\rangle$ (except for the value $\langle n\rangle = 2.7$, printed as 2.9, but which can safely be assumed to be a printing error). In Fig. 8 we compared their $f(n)$ with the GCMC simulations at 300 K. We find a reasonable agreement between the simulations and their experimental data.

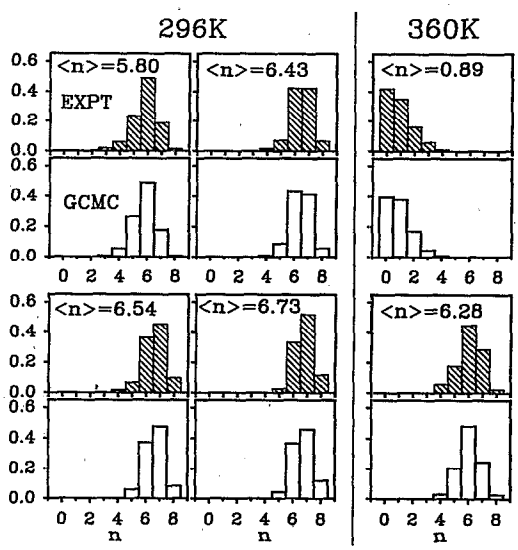

FIG. 7. The same as for Fig. 5 except that these are the other four samples at high loading. Two of the ten samples are shown here at 360 K to demonstrate that the GCMC simulations at 360 K are also in very good agreement with experimental equilibrium distributions at 360 K.

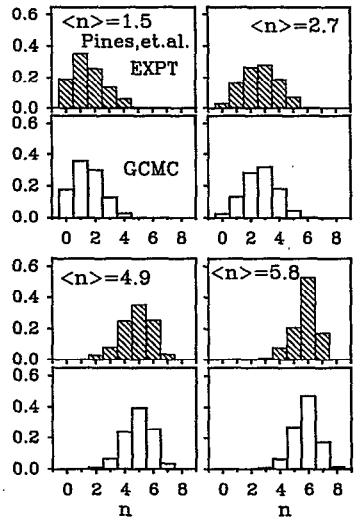

FIG. 8. The $f(n)$ reported by Pines *et al.* (Ref. 27) at 300 K are compared with the $f(n)$ from the GCMC simulations at this temperature.

We have already shown that the measured distributions of the Xe atoms among the alpha cages of zeolite NaA cannot be reproduced by either the hypergeometric distribution or the continuum model.[25] Since we have data for the full range of loading conditions, and since the GCMC results reproduce the $f(n)$ data very well over the entire range, it should be possible to derive from experiment and simulations what the expected $f(n)$ distribution ought to be for any value of $\langle n \rangle$ in the Xe in the dehydrated zeolite NaA system. In so doing, it may also reveal in what fundamental ways the actual distribution differs from the hypergeometric distribution, and provide insight into the expected distributions for other zeolites where the individual clusters cannot be observed. For a specific n, the curve describing the change of $f(n)$ with $\langle n \rangle$ would generally be zero at $\langle n \rangle$ values much less than n, also zero at $\langle n \rangle$ values much greater than n, and will be increasing as n approaches $\langle n \rangle$ from both directions. In the hypergeometric distribution, the curves are related by symmetry, the $f(0)$ and the $f(8)$ are mirror images; in general, $f(n)$ and $f(8-n)$ are mirror images, if the number of sites is 8. The actual distribution deviates from the hypergeometric in the following ways: The curves are no longer related by symmetry, $f(1)$ and $f(7)$ are very different in shape, for example. Also, the fraction of cages containing seven atoms for the loading $\langle n \rangle = 7$ is much greater than statistical, whereas the fraction of cages containing one atom for the loading $\langle n \rangle = 1$ is less than statistical. Figure 9 shows the actual and simulated $f(n)$ vs $\langle n \rangle$ curves at room temperature and at 360 K, compared to the $f(n)$ vs $\langle n \rangle$ for the statistical distribution (which does not change with temperature, of course). For the statistical distribution, the envelope formed by the highest probability of finding a cluster Xe_k passes through the points $\langle n \rangle = k$ and is symmetrical for the hypergeometric distribution. This envelope in the actual case is very unsymmetrical, having its minimum not at $n=4$ but at $n=3$, and the highest probability of finding a cluster Xe_k in

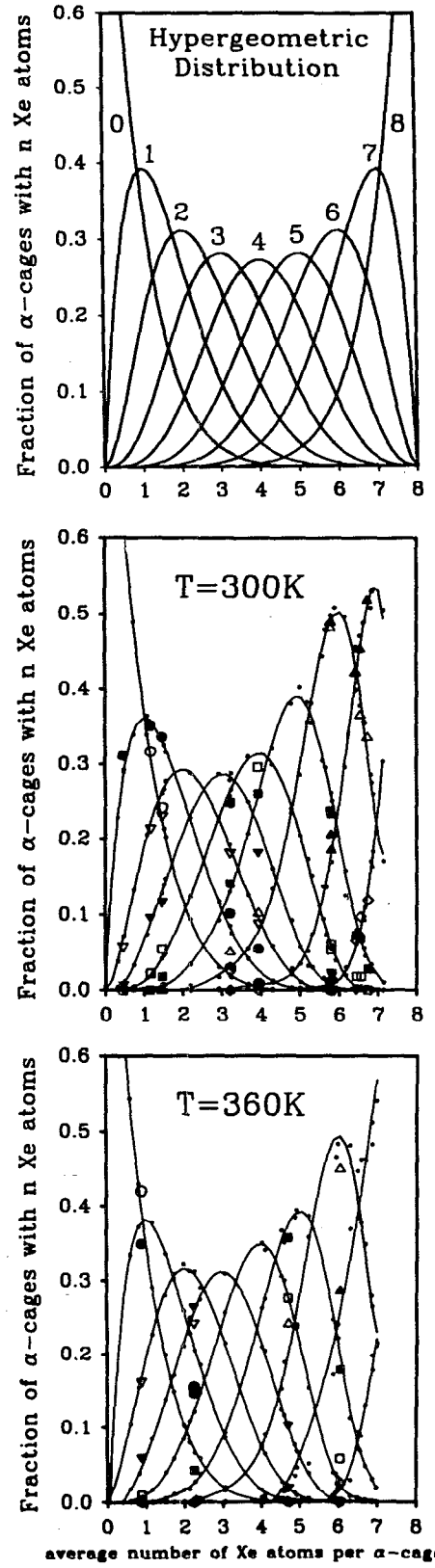

FIG. 9. The $f(n)$ change with loading in a systematic way. These are the results of the GCMC simulations at 300 and 360 K. Experimental values are shown in open and filled symbols. The $f(n)$ predicted by the hypergeometric distribution are also given here for comparison.

a sample is not found at $\langle n\rangle = k$, but at a slightly smaller value of $\langle n\rangle$, especially for the larger clusters. The 360 K data has the same asymmetry, and contrary to expectation, was not any closer to the statistical distribution in the details. For example, the highest probability of finding the cluster Xe_5 in a sample is greater than predicted by the statistical distribution and occurs at a value of $\langle n\rangle$ slightly less than 5. In the hypergeometric distribution one can also count the number of "holes" since this distribution is for a fixed number of sites. If we also think in terms of holes for the actual case, and compare with the hypergeometric distribution, we find

HYPERGEOMETRIC	ACTUAL
$\{f(n)$ vs $\langle n\rangle\} = \{f(8-n)$ vs $8-\langle n\rangle\}$ for all n	$\{f(n)$ vs $\langle n\rangle\} < \{f(8-n)$ vs $8-\langle n\rangle\}$ for $n<4$ $\{f(n)$ vs $\langle n\rangle\} > \{f(8-n)$ vs $8-\langle n\rangle\}$ for $n>4$

Just as for the hypergeometric distribution, the half-width of $f(n)$ vs $\langle n\rangle$ increases with increasing n for $n \leqslant 4$ and decreases with increasing n for $n \geqslant 4$. The maximum value of $f(n)$ appears to become greater for the higher temperature for n greater than 4.

Let us now consider the distribution of the Xe atoms between the adsorbed phase in the intrazeolitic regions and the gas phase. The grand canonical ensemble permits the simulation of the equilibrium between these phases. The adsorption isotherm is given by $\langle N\rangle$ which is directly obtained in the grand canonical ensemble. We present the simulated adsorption isotherms in Fig. 10. There are only a limited number of measurements because the gas peak is not observable in the samples of $\langle n\rangle = 3.94$ or lower. Nevertheless, for the remaining samples, the experimental values are in very good agreement with the simulations.

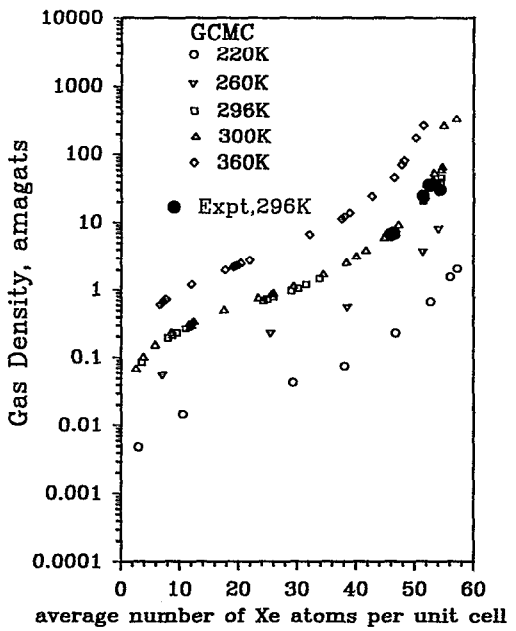

FIG. 10. The adsorption isotherms obtained from the GCMC simulations are shown here for several temperatures. The experimental values are for all samples having $\langle n\rangle > 3.94$ in equilibrium at 296 K. These are the only ones for which the gas peak could be observed and the gas density determined reliably from its chemical shift. An amagat is 2.688×10^{19} molecules per cm^3, i.e., the density of an ideal gas at 273.16 K and 1 atm.

B. The ^{129}Xe chemical shifts

The ^{129}Xe nuclear magnetic shielding is calculated relative to the free Xe atom and the measured quantity is also the shielding relative to the free Xe atom, obtained experimentally by extrapolating the resonance frequencies of the samples of various densities of xenon gas to the zero density limit. Our goal was to understand the magnitudes of the shielding differences between the clusters and not their absolute magnitudes. However, fortunately (perhaps fortuitously) the average shielding for a single Xe in the zeolite is represented well enough by our sum of pairwise shielding functions as a function of position inside the alpha cage, so that we can compare the absolute magnitudes, not just the increments. The incremental shifts had been previously explained qualitatively, entirely on the basis of the shape of the intermolecular shielding function.[25] Therefore, it was not unexpected that GCMC simulations would provide the correct qualitative behavior. The average shieldings of the Xe_n clusters at 300 K are shown in Table II and Fig. 11, where it can be seen that the agreement with experiment is very good, although not, we believe, within our experimental errors. Note that the GCMC simulations reproduce the gradual increase in the increments in going from Xe_1 to Xe_5. Furthermore, the large chemical shift increment between Xe_6 and

TABLE II. The NMR chemical shielding of Xe_n clusters from experiment and GCMC simulations.

	$\langle\sigma(Xe_n)-\sigma$(free atom)$\rangle$		Increments	
n	Expt.[a]	GCMC	Expt.[a]	GCMC
1	−74.8	−77.2		
2	−92.3	−92.6	17.5	15.5
3	−111.7	−109.6	19.4	17.0
4	−133.2	−129.9	21.5	20.3
5	−158.4	−155.4	25.2	25.5
6	−183.4	−184.2	25.1	28.9
7	−228.3	−226.0	45.1	41.7
8	−272.3	−269.7	43.7	43.7

[a]Reference 25.

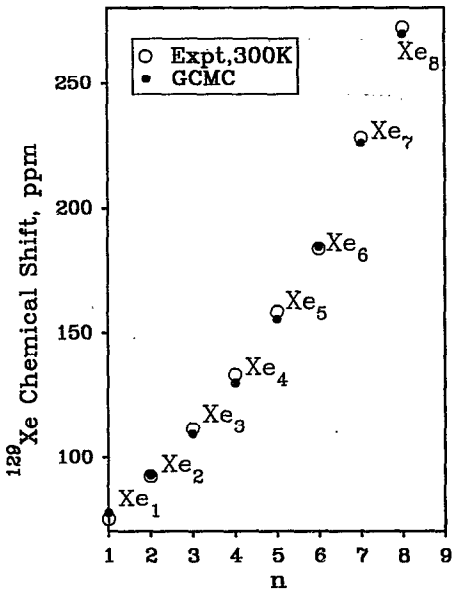

FIG. 11. The experimental ^{129}Xe chemical shifts for Xe_1 through Xe_8 at 300 K, compared with the GCMC results.

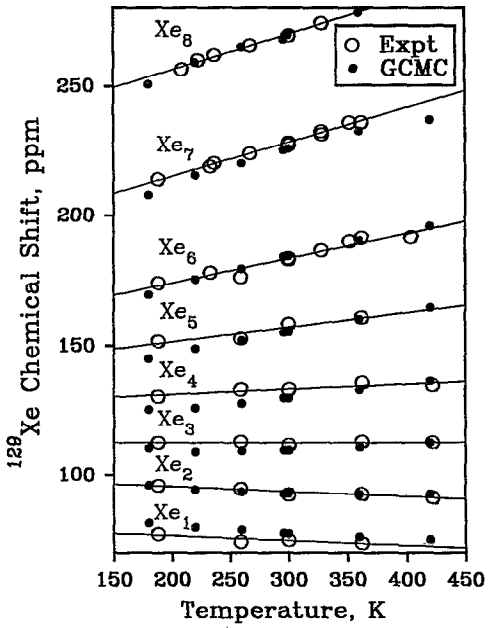

FIG. 12. The temperature dependence of the ^{129}Xe chemical shifts of the clusters are shown together with the GCMC results. The lines are linear least-squares fit descriptions of the experimental data.

Xe_7 and between Xe_7 and Xe_8 are reproduced. Note that no structural information has been introduced into the simulation, other than the structure of the zeolite lattice itself from x-ray and neutron diffraction. No specific structures were assigned to the clusters, the configurations sampled in the simulations are dictated entirely by the summation over pairwise potentials. That the large incremental shifts are reproduced by the simulations indicates that the system is reasonably mimicked by the model potentials used here. Since the ^{129}Xe shielding function is a smooth function, having no steps or unusual features, then the distribution of the configurations of Xe_6, Xe_7, and Xe_8, as they are determined by the Xe–Xe pairwise interactions and the imposed rigid structure of the alpha cage must themselves be responsible for the observed and simulated jumps in chemical shifts. We will examine the structure of the clusters, as revealed by the simulations, in the following paper.

A more stringent test is the temperature dependence of the ^{129}Xe chemical shifts. This too had been explained qualitatively before,[25] so the GCMC simulation was expected to reproduce the qualitative behavior of the systematic change in the slope (change in the ^{129}Xe chemical shift upon increasing temperature) in going from Xe_1 to Xe_8. It does indeed, and the results are shown in Fig. 12. The GCMC simulations do provide the correct trends and very nearly the correct temperature coefficients for all clusters. Again it should be noted that these are absolute quantities and neither the magnitude nor the temperature dependence of each cluster shift are adjusted relative to experiment in any way. A physical understanding of the temperature dependence of the cluster shifts can be obtained from the examination of the shielding function dependence on intermolecular distance. For the single Xe atom in an alpha cage, the only shielding contributions come from the proximity of the Xe atom to the oxygen atoms and the counterions of the zeolite. At low temperatures, the Xe atom is found close to the wall of the alpha cage, thereby sampling the very deshielded regions of the shielding functions σ(Xe–O) and σ(Xe–Na^+). At higher temperatures, the Xe atom can spend a larger fraction of its time farther away from the wall, sampling the less deshielded parts of the shielding functions. These translate to an average chemical shift that is decreasing with increasing temperature. This Xe–zeolite contribution to the chemical shift is present for all the clusters. However, when there is one other Xe atom in the alpha cage, the Xe–Xe contributions to the shielding begin to contribute. As the temperature increases, the short-range highly deshielded regions of the σ(Xe–Xe) which are in the repulsive regions of the U(Xe–Xe) function are sampled more often, thereby leading to a contribution to the chemical shift which increases with temperature for the larger clusters compared to the smaller ones.

The above discussion provides a guide to the significance of the Xe chemical shifts in microporous solids. What we have in the average ^{129}Xe chemical shift of the Xe_n cluster is an indirect measure of the distribution of the n Xe atoms within one alpha cage for any given temperature. This information is encoded in the value of the average chemical shift, which is a convolution of the Xe shielding sensitivity to intermolecular distances [r(Xe–Xe) primarily] in an Xe_n cluster and the relative weights of the various Xe_n configurations. The average ^{129}Xe shielding in Xe_n is therefore a good test of the adequacy of the σ(Xe–Xe) shielding function and the accuracy of the one-body distribution, and more importantly, the pair distribution function of the Xe atoms within an alpha cage. The very good agreement between the absolute chemical shifts of the clusters and their change with temperature leads us to believe that we may have a reasonable description of the configurations sampled by the Xe_n

clusters at most temperatures in the range 180 to 420 K. It should be noted that the agreement between experiment and GCMC averages are worst at the lowest temperatures. This may indicate that the many-body terms in the Xe–Xe shielding and perhaps in the interaction energy may no longer be negligible at these temperatures. The neglect of many-body corrections while using a realistic two-body Xe–Xe potential will cause problems in the average configurational energy at high loading. This is precisely the reason why the Lennard-Jones form in Fig. 3, fitted to condensed phase properties, is commonly used. It compensates for the lack of many-body corrections in simulations and describes the liquid and solid properties well.

It is also of some interest to examine the ^{129}Xe shielding in the minimum energy configurations. The zeolite contributions to the shielding differs from one Xe to another in the same cluster configuration, depending on the proximity to Na^+ ions and O atoms. For a single Xe atom in the alpha cage there is a spread of -93 to -100 ppm depending on the adsorption site. Let us consider Xe_8 as an example. We found six minimum energy configurations. The individual nuclei can be in quite different environments (50 to 120 ppm spread among the 8 Xe nuclei in a cluster), but the average of the NMR shielding over all eight Xe nuclei does not vary greatly (23 ppm spread, of which 7.7 ppm are in the zeolite contributions and 15.5 ppm in the Xe–Xe contributions). Furthermore, it is of interest that although each Xe is with seven other Xe atoms in the cavity, only four of them contribute significantly to its shielding, while three others contribute in most cases less than 0.1 ppm. This confirms what we already know: that the NMR chemical shift is a very local electronic property. Only the Xe atoms that are "touching" the one in question have non-negligible contributions to the shift. When it becomes possible to populate the center of the cavity (very high temperatures and Xe pressures) the number of neighboring Xe atoms at short distances will be larger yet and the ^{129}Xe chemical shift in Xe_8 will be extremely large.

Examination of the ^{129}Xe shieldings in the minimum energy configurations provides a contrast with proper averaging. If only the minimum energy configurations were considered, the chemical shifts that would have been predicted would not have reflected experiment accurately. The averaging is crucial to getting the proper weighting of all possible configurations, not just the local minima in the configuration space of the cluster. For example, we find that the lowest-energy structures give shieldings which are -99.1, -104.4, -132.9, -148.5, -160.0, -162.3, -184.5, and -216.4 ppm, respectively, for the Xe_1, Xe_2,...,Xe_8 clusters. These provide chemical shielding increments that are not at all like the ones obtained from experiment or from the GCMC averages. Further, the 11 Xe_1 minimum energy sites range in chemical shielding from -92.6 to -100.6 ppm, whereas the GCMC average at 300 K is -77.2 ppm. Six local minima on the Xe_8 configuration space have Xe_8 chemical shieldings ranging from -216.4 to -239.3 ppm whereas the GCMC average at 300 K is -269.7 ppm. The downfield shift for Xe_1 is greater and that for Xe_8 is less than the proper weighting given by the GCMC simulations at 300 K. Clearly, taking Boltzmann weighted averages of the shieldings corresponding to multiple local minima in the configuration space of a cluster is not a valid approach. In this particular system, this would lead to results that are not at all like the proper GCMC averages. This means that consideration of possible low-energy structures of Xe_n clusters within the zeolite cages to explain the observed chemical shift increments is not a useful approach.

V. CONCLUSIONS

We have several experimental measures of the distribution of Xe atoms in zeolite NaA. The distribution between the intrazeolitic regions and the free gas is provided by the adsorption isotherm. The distribution of Xe atoms among the alpha cages is provided by the $f(n)$, the fractions of alpha cages containing Xe_n, $n=0$ to 8. Third, the distribution of the n Xe atoms within one alpha cage (or what one might think of as the weights of the various cluster configurations) are encoded within the average chemical shift of the Xe_n cluster. The temperature dependences of these three types of distribution are, of course, revealed in the temperature dependences of these three observables. The GCMC simulations reported here have reproduced quantitatively all three observables (although we believe that the chemical shifts are not matched within our own experimental errors). The parameters in the potential functions or the shielding functions have not been fitted to these experiments. One of the advantages of this study is that comparisons can be made with several properties that have been measured in the same samples with the same set of GCMC simulations with no changes in the parameters of the model and with no fitting to any experiments.

This is the first computer simulation of the average ^{129}Xe chemical shifts in a zeolite, and the first to demonstrate quantitative agreement with the experimental equilibrium distribution of Xe atoms among the cavities of a zeolite. We believe that the distribution of the Xe atoms among the alpha cages for a given $\langle n \rangle$ is well reproduced by the GCMC simulations because we have a fairly good representation of the internal structure of the alpha cage. We are fortunate in that this particular zeolite has been very well characterized so that the location of every atom and ion has been established by x-ray and neutron diffraction. We have used these coordinates to represent the zeolite in the simulation so that the corrugation of the internal surface is very well represented by the use of Lennard-Jones potentials for the Xe–O and Xe–Na^+ interactions. The average chemical shifts of the individual Xe_n clusters and their temperature dependence are also reasonably well represented because we are using a ^{129}Xe shielding function that has been successful in reproducing the gas phase intermolecular shifts in pure xenon gas and a good two-body potential function for Xe–Xe interactions samples the shielding surface accurately. The corrugation of the cage and its internal space being set by the zeolite structure, the Xe atoms within an alpha cage are appropriately constrained in the distances that they can assume relative to each other. It is these factors that lead to a successful simulation despite the fact that there are no adjustable parameters of any kind. For this particular system, the nonadditive terms in the energy and shielding, which have been

completely neglected in this study, do not appear to play an important role (except perhaps in the cluster shifts at very low temperatures). We are continuing to investigate the nonadditive terms in both the energy and the shielding. The Xe–zeolite shielding function used here is only a first approximation and requires further *ab initio* studies. Ultimately, it may be possible to reproduce the Xe chemical shifts in the limit of zero loading (Xe–zeolite intermolecular shifts only) for several zeolites. For this, we will probably need to have the Xe–O effective potential function and the Xe–O shielding function depend on the Si/Al ratio in a systematic way. To this end, we are carrying out *ab initio* calculations of nuclear shielding of a rare gas atom in the presence of clusters of the type $Na_2^+[(SiO_2H)_2(AlO_2H)_2(OH)_4]^{2-}$, $Na_3^+[(SiO_2H)_3(AlO_2H)_3(OH)_6]^{3-}$, and the corresponding highly siliceous and aluminated clusters.

ACKNOWLEDGMENTS

This research was funded by the National Science Foundation (Grant No. CHE92-10790). This work would not have been possible without the generous hospitality of Professor John Rowlinson who hosted C.J.J.'s visit to the Physical Chemistry Laboratory, Oxford University where she learned how to do GCMC simulations. We are grateful to E. Brian Smith for suggesting the Maitland–Smith potential form used in this work. Angel C. deDios carried out the Ar shielding calculations in Ar–OH_2. The results reported here were presented at the Symposium on Statistical Mechanics of Fluids, March 30–31, 1993 in honor of the contributions of John Rowlinson to the field, and in the Symposium on Molecules in Restricted Geometries, ACS National Meeting in Denver, March 28–30, 1993.

[1] *Molecular Dynamics in Restricted Geometries*, edited by J. Klafter and J. M. Drake (Wiley, New York, 1989).
[2] *Guidelines for Mastering the Properties of Molecular Sieves: Relationship between the Physicochemical Properties of Zeolitic Systems and their Low Dimensionality*, edited by D. Barthomeuf, E. G. Derouane, and W. Holderich, NATO ASI Ser. 221 (Plenum, New York, 1989).
[3] G. Engelhardt and D. Michel, *High Resolution Solid State NMR of Silicates and Zeolites* (Wiley, Chichester, 1987).
[4] *Introduction to Zeolite Science and Practice*, edited by H. van Bekkum, E. M. Flanigen, and J. C. Jansen (Elsevier, Amsterdam, 1991).
[5] *Shape Selective Catalysis in Industrial Applications*, edited by N. Y. Chen, W. E. Garwood, and F. G. Dwyer (Marcel Dekker, New York, 1989).
[6] Proceedings of ZEOCAT90, Leipzig, August 1990; *Catalysis and Adsorption by Zeolites* (Elsevier, Amsterdam, 1990).
[7] Studies in Surface Science and Catalysis, *Recent Advances in Zeolite Science*, edited by J. Klinowski and P. J. Barrie (Elsevier, Amsterdam, 1989), Vol. 52.
[8] A. K. Jameson, C. J. Jameson, and H. S. Gutowsky, J. Chem. Phys. **53**, 2310 (1970).
[9] C. J. Jameson, A. K. Jameson, and S. M. Cohen, J. Chem. Phys. **59**, 4224 (1973).
[10] C. J. Jameson, Bull. Magn. Reson. **3**, 3 (1980).
[11] C. J. Jameson, Chem. Rev. **91**, 1375 (1991).
[12] T. R. Stengle, N. V. Reo, and K. L. Williamson, J. Phys. Chem. **85**, 3772 (1981).
[13] T. R. Stengle, S. M. Hosseini, and K. L. Williamson, J. Solut. Chem. **15**, 777 (1986).
[14] J. Fraissard and T. Ito, Zeolites **8**, 350 (1988).
[15] P. J. Barrie and J. Klinowski, Prog. NMR Spectrosc. **24**, 91 (1992).
[16] T. Ito and J. Fraissard, J. Chem. Phys. **76**, 5225 (1982).
[17] J. Fraissard, Z. Phys. Chem. **152**, 159 (1987).
[18] T. T. P. Cheung, C. M. Fu, and S. Wharry, J. Phys. Chem. **92**, 5170 (1988).
[19] B. F. Chmelka, J. G. Pearson, S. B. Liu, L. C. de Menorval, and A. Pines, J. Phys. Chem. **95**, 303 (1991).
[20] A. Gedeon, T. Ito, and J. Fraissard, Zeolites **8**, 376 (1988).
[21] E. G. Derouane and J. B. Nagy, Chem. Phys. Lett. **137**, 341 (1987).
[22] J. Demarquay and J. Fraissard, Chem. Phys. Lett. **136**, 314 (1987).
[23] D. W. Johnson and L. Griffiths, Zeolites **7**, 484 (1987).
[24] J. A. Ripmeester and C. I. Ratcliffe, J. Phys. Chem. **94**, 7652 (1990).
[25] C. J. Jameson, A. K. Jameson, R. Gerald II, and A. C. de Dios, J. Chem. Phys. **96**, 1676 (1992).
[26] C. J. Jameson, A. K. Jameson, R. Gerald II, and A. C. de Dios, J. Chem. Phys. **96**, 1690 (1992).
[27] B. F. Chmelka, D. Raftery, A. V. McCormick, L. C. de Menorval, R. D. Levine, and A. Pines, Phys. Rev. Lett. **66**, 580 (1991); **67**, 931 (1991).
[28] J. Guemez and S. Velasco, Am. J. Phys. **55**, 154 (1987).
[29] J. S. Rowlinson and G. B. Woods, Physica A **164**, 117 (1990).
[30] G. B. Woods, A. Z. Panagiotopoulos, and J. S. Rowlinson, Mol. Phys. **63**, 49 (1988).
[31] G. B. Woods and J. S. Rowlinson, J. Chem. Soc. Faraday Trans. 2 **85**, 765 (1989).
[32] S. Yashonath, Chem. Phys. Lett. **177**, 54 (1991).
[33] S. Yashonath, J. Phys. Chem. **95**, 5877 (1991).
[34] S. Yashonath and P. Santikary, Phys. Rev. B **45**, 1095 (1992).
[35] R. L. June, A. T. Bell, and D. N. Theodorou, J. Phys. Chem. **94**, 8232 (1990).
[36] S. D. Pickett, A. K. Nowak, J. M. Thomas, B. K. Peterson, J. E. P. Swift, A. K. Cheetham, C. J. J. den Ouden, B. Smit, and M. F. M. Post, J. Phys. Chem. **94**, 1233 (1990).
[37] A. V. Kiselev and P. Q. Du, J. Chem. Soc. Faraday Trans. 2 **77**, 1 (1981).
[38] A. G. Bezus, A. V. Kiselev, A. A. Lopatkin, and P. Q. Du, J. Chem. Soc. Faraday Trans. 2 **74**, 367 (1978).
[39] P. R. van Tassel, H. T. Davis, and A. V. McCormick, Mol. Phys. **73**, 1107 (1991).
[40] P. R. van Tassel, H. T. Davis, and A. V. McCormick, Mol. Phys. **76**, 411 (1992).
[41] A. V. Vernov, W. A. Steele, and L. Abrams, J. Phys. Chem. **97**, 7660 (1993).
[42] P. R. van Tassel, H. T. Davis, and A. V. McCormick, J. Chem. Phys. **98**, 8919 (1993).
[43] J. J. Pluth and J. V. Smith, J. Am. Chem. Soc. **102**, 4704 (1980).
[44] J. M. Bennett, C. S. Blackwell, and D. E. Cox, in *Intrazeolite Chemistry*, edited by G. D. Stucky and F. G. Dwyer, ACS Symp. Series 218 (American Chemical Society, Washington, D.C., 1983), p. 143.
[45] *International Tables for Crystallography*, International Union of Crystallography (Reidel, Dordrecht, 1987), Vol. A.
[46] G. B. Woods, D.Phil. thesis, Oxford University (1989).
[47] M. Schmeits and A. A. Lucas, Prog. Surf. Sci. **14**, 1 (1983).
[48] C. J. Jameson and A. C. de Dios, J. Chem. Phys. **98**, 2208 (1993).
[49] R. A. Aziz and M. J. Slaman, Mol. Phys. **57**, 825 (1986).
[50] G. C. Maitland, M. Rigby, E. B. Smith, and W. A. Wakeham, *Intermolecular Forces, their Origin and Determination* (Clarendon, Oxford, 1981).
[51] C. J. Jameson and A. C. de Dios, J. Chem. Phys. **97**, 417 (1992).
[52] M. P. Allen and D. J. Tildesley, *Computer Simulation of Liquids* (Clarendon, Oxford, 1987).
[53] G. E. Norman and V. S. Filinov, High Temp. USSR **7**, 216 (1969).
[54] M. Mezei, Mol. Phys. **61**, 565 (1987).
[55] J. J. Nicolas, K. E. Gubbins, W. B. Streett, and D. J. Tildesley, Mol. Phys. **37**, 1429 (1979).